



HAL
open science

Oscillation mode variability in evolved compact pulsators from Kepler photometry. II. Comparison of modulation patterns between raw and corrected flux

Weikai Zong, Stephane Charpinet, Gerard Vauclair

► **To cite this version:**

Weikai Zong, Stephane Charpinet, Gerard Vauclair. Oscillation mode variability in evolved compact pulsators from Kepler photometry. II. Comparison of modulation patterns between raw and corrected flux. *The Astrophysical Journal*, 2021, 10.3847/1538-4357/ac1b2c . hal-03400960

HAL Id: hal-03400960

<https://hal.science/hal-03400960v1>

Submitted on 28 Oct 2021

HAL is a multi-disciplinary open access archive for the deposit and dissemination of scientific research documents, whether they are published or not. The documents may come from teaching and research institutions in France or abroad, or from public or private research centers.

L'archive ouverte pluridisciplinaire **HAL**, est destinée au dépôt et à la diffusion de documents scientifiques de niveau recherche, publiés ou non, émanant des établissements d'enseignement et de recherche français ou étrangers, des laboratoires publics ou privés.

Oscillation mode variability in evolved compact pulsators from *Kepler* photometry. II. Comparison of modulation patterns between raw and corrected flux

WEIKAI ZONG,¹ STÉPHANE CHARPINET,² AND GÉRARD VAUCLAIR²

¹*Department of Astronomy, Beijing Normal University, Beijing 100875, P. R. China*

²*IRAP, Université de Toulouse, CNRS, UPS, CNES, 14 avenue Edouard Belin, F-31400, Toulouse, France*

(Received —; Revised —; Accepted —)

Submitted to ApJ

ABSTRACT

We present the second results of an ensemble and systematic survey of oscillation mode variability in compact pulsators observed with the original *Kepler* mission. Two types of flux calibrations, raw and corrected, collected on two hot B subdwarf stars, KIC 2438324 and KIC 11179657, are thoroughly examined with the goal to evaluate the difference of patterns when oscillation modes modulate in amplitude (AM) and frequency (FM). We concentrate on AMs and FM s occurring in seven multiplet components in each star as representative frequencies. The analysis shows that FM measurements are independent of the flux calibration we choose. However, if flux contamination by nearby stars is large, AMs may be significantly different between raw and corrected flux. In addition, AMs suffer, to some extent, from systematic modulation pattern which is most likely induced by instrumental effects and differs from one star to another. Our results indicate that stars with no contamination are better candidates to quantitatively compare modulation patterns with theory and should be given a higher priority for such studies, since light contamination will destroy real amplitude modulation patterns.

Keywords: technique: photometric — stars: evolved variables — stars: oscillations

1. INTRODUCTION

This series of papers is devoted to an ensemble and systematic survey of oscillation mode variability in pulsating hot B subdwarf (sdB) and white dwarf stars using *Kepler*'s photometry, particularly for stars with over two years of monitoring. We recall, in the first paper of this series (Zong et al. 2018, hereafter Paper I), that a particular sdB star, KIC 3527751, was thoroughly analyzed with a total of 204 frequencies resolved from a nearly contiguous 38-month long light curve. We investigated mode variability and stability for 143 frequencies with relatively large amplitudes (i.e., with acceptable significance level in just a portion of the entire light curve) and found that all of those frequencies show evident variations, with regular or irregular modulation patterns. We showed that these variations are likely reminiscent of nonlinear weak mode interactions predicted by the resonant mode coupling formalism (e.g., Buchler et al. 1997), where the oscillation mode under certain resonance conditions may exhibit temporal amplitude modulations (AM) and frequency

modulations (FM) of various patterns or stay stable over time. Such observed modulation patterns will eventually be compared to theoretical ones, once calculations of nonlinear coupling coefficients involving many modes (Buchler et al. 1995) will become available. The direct comparison of AMs and FM s has only been achieved for a few pulsating stars (see, e.g., Kovacs & Buchler 1989), thus far. Therefore, the current and most urgent step is to provide intrinsic AM and FM measurements as this opportunity is now offered by *Kepler*. Recent results show that pulsating sdB and white dwarf stars may be among the best candidates on this front (see, e.g., Zong et al. 2016a).

In the original *Kepler* field, the satellite collected exquisite high-quality photometry for eighteen pulsating sdB stars and six white dwarf stars (see Paper I, and references therein). Most of these objects have been intensively observed in the competitive short-cadence (58.85 s) mode over a duration of two years due to their rapid oscillation timescales (from a few minutes to a few hours) and scientific significance. *Kepler* pipelines provide available light curves in two forms: the “raw” flux, also referred to as the Simple Aperture Photometry (SAP), and the “corrected” flux, also called Pre-search

Data Conditioning SAP (PDCSAP; see, e.g., [Jenkins et al. 2010](#)). The latter data impose cotrending basis vectors to correct the discontinuities and contamination of raw flux over different quarters. Although the corrected data contain cleaner light curves, this process may bring extra or modify intrinsic astrophysical signatures of some particular targets (see [Murphy 2012](#)). In the context of precisely characterizing modulation patterns in oscillation modes, the impact of using two different types of flux has never been examined. Concretely, evaluating these differences for some particular stars might be necessary before attempting quantitative comparisons with theoretical calculations.

With this purpose in mind, we chose two long-period g -mode pulsating sdB stars, KIC 2438324 and KIC 11179657, as representative objects to check if using two different kinds of fluxes leads to significant differences in the modulation patterns. KIC 2438324, or B4 in NGC 6791, has a mean brightness $Kp = 18.267$, effective temperature $T_{\text{eff}} = 24\,786 \pm 655$ K and surface gravity $\log g = 5.30 \pm 0.09$ dex ([Reed et al. 2012](#)). The detection of pulsations in this very faint star required the acquisition of over six months of *Kepler* photometry ([Pablo et al. 2011](#)), which established its variability. KIC 11179657, or USNO-A2.0 1350-10140904, has a mean brightness $Kp = 17.065$, $T_{\text{eff}} = 26\,000 \pm 800$ K and $\log g = 5.14 \pm 0.13$ dex ([Østensen et al. 2010](#)). For that star, the presence of pulsations was revealed during the first year survey phase, on the basis of a ~ 30 days light curve ([Østensen et al. 2010](#)). Both stars are found to be members of a binary system with low-mass main-sequence companions, and both are not synchronized, as suggested by the seismic rotation periods which are longer than the orbital periods ([Pablo et al. 2011, 2012](#)).

In this paper, we first assess the robustness of our error estimates for the amplitude, frequency and phase from quantitative tests in Section 2. Section 3 is dedicated to the thorough analysis of the *Kepler* photometry collected for these two sdB stars. The extracted modulation patterns for representative mode frequencies and comparisons with the orbital signals are presented in Section 4 and 5, followed by a discussion in Section 6 and a conclusion.

2. TESTING THE ROBUSTNESS OF ERROR ESTIMATES

Considering the importance of error estimates for our scientific goals, we made a series of simulations to assess their robustness for frequencies extracted from the *Kepler* photometry. These tests constitute an extension of those described in ([Zong et al. 2016b](#)). A variant of such simulations was also carried out recently by [Silvotti et al. \(2018\)](#), in order to check the reliability of errors for measured frequencies that suggest the presence of a giant planet around V391 Peg.

We briefly describe how this series of simulations was done: 1) 50 artificial light curves containing Gaussian white noise were generated using a time sampling of 58.85 s and a duration of 200 days without interruption; 2) in each light curve, 1 000 frequencies of constant amplitude (details are provided in [Zong et al. 2016b](#)) were injected, with amplitude values varying from light curve to light curve; 3) The code FELIX¹ was used to detect and extract automatically the injected frequencies in each simulated light curve; 4) two estimates for the normalized errors were calculated, using different methods. One method was to derive analytically the errors following [Montgomery & Odonoghue \(1999, hereafter MO99\)](#), with the relations for amplitude, frequency and phase uncertainties :

$$\sigma_A = \sqrt{2/N} \sigma_m, \quad (1a)$$

$$\sigma_f = \frac{\sqrt{3}}{\pi T} \frac{\sigma_A}{A}, \quad (1b)$$

$$\sigma_\phi = \sigma_A/A, \quad (1c)$$

where N and T are the number of data points and the total duration of the time-series, respectively. A and σ_m are the measurable amplitude of a frequency peak and the root-mean-square deviation of the magnitude in the light curve, respectively. The other method which was used thus far in the code FELIX directly measures σ_A as the median value of the noise around a detected peak in the Fourier transform of the light curve. σ_f is then calculated with equation 1b) and σ_ϕ comes from the covariance matrix of the nonlinear least-square fit of the light curve. The normalized errors for the amplitude, frequency and phase are defined as

$$\Delta_A = (A_{\text{pre}} - A_{\text{inj}})/\sigma_A, \quad (2a)$$

$$\Delta_f = (f_{\text{pre}} - f_{\text{inj}})/\sigma_f, \quad (2b)$$

$$\Delta_\phi = (\phi_{\text{pre}} - \phi_{\text{inj}})/\sigma_\phi. \quad (2c)$$

respectively. Subscripts “pre” and “inj” refer to prewhitened (measured) and injected values.

Figure 1 shows the results of our simulations from a total of 50 000 injected sinusoidal waves. By using normalized errors, one expects to obtain normal distributions of zero mean and standard deviation one, $N \sim (0, 1)$, if the values of σ_A , σ_f , and σ_ϕ are correctly estimated. A narrower distribution than $N \sim (0, 1)$ gives an overestimation of error. We clearly see that all prewhitened values are very similar to the injected ones, as revealed by the vertical dashed lines near the center. This indicates that there is no bias in the frequency extraction method. Amplitude and frequency uncertainties evaluated from MO99 equations and from our implemented

¹Frequency Extraction for LIghtcurve eXploitation (see details in [Charpinet et al. 2010, 2011; Zong et al. 2016b](#))

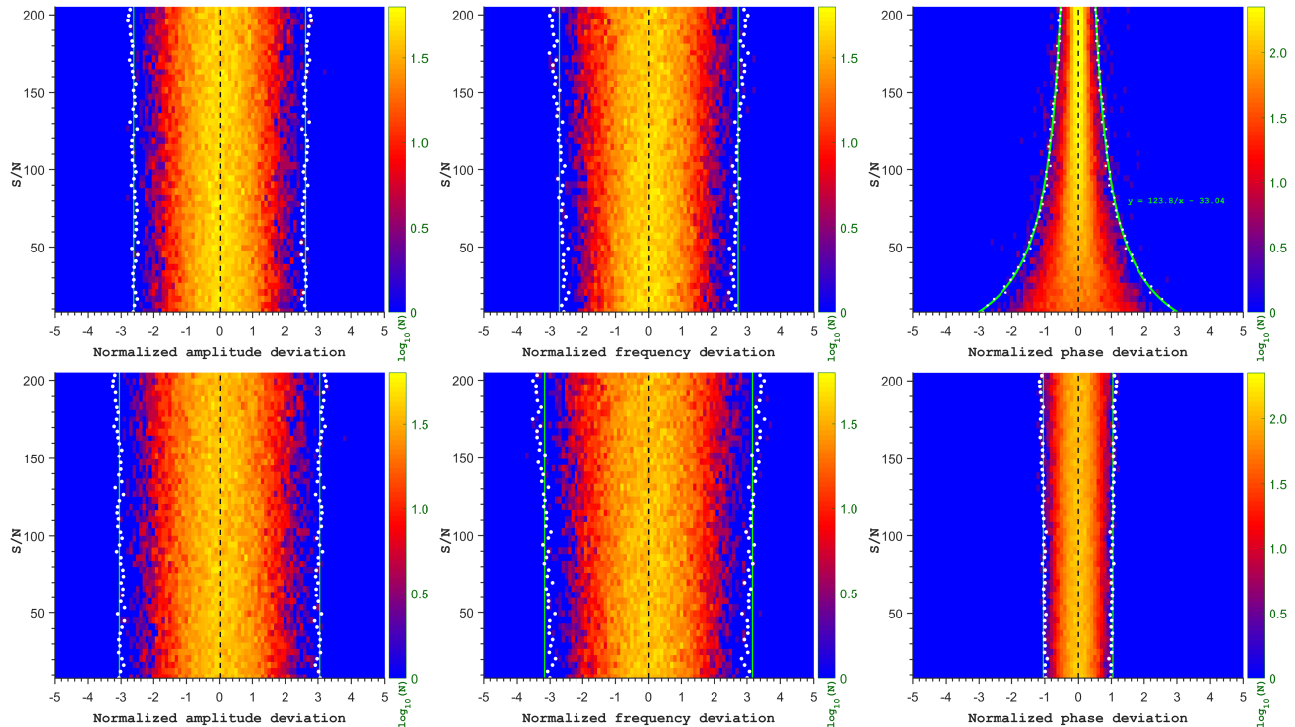


Figure 1. Distribution of normalized amplitude, frequency and phase deviations between the extracted and injected signals (from left to right panels). Top panels correspond to the default method to compute errors used with the code FELIX (see text) and bottom panels correspond to errors determined analytically following [Montgomery & Odonoghue \(1999\)](#). The (central) dashed lines indicates the mean deviations calculated from the distribution, which are all very close to zero. The dotted curves indicate $\pm 3\times$ the standard deviations as a function of S/N. In all panels except the top-right one, S/N-averaged values for 3σ are represented by vertical solid lines. For the top-right panel, the solid curve is fitted using a reciprocal model. Color coding refers to the occurrence (using a logarithmic scale) of measurements at specific deviation and S/N values.

method are both found to be in agreement with the normal distribution in general. However, ours slightly overestimates σ_A and σ_f by about 10% and 5%, while MO99 slightly underestimate these errors by about 2% and 5%, respectively. We note that there is possibly a slight dependence to S/N of the normalized frequency deviations (i.e., the dashed lines at the low and high S/N ends stand at two sides of the solid vertical lines). The phase deviations, however, show two different behaviors. The one derived from the covariance matrix of the nonlinear fit presents a clear dependence on S/N as it become gradually overestimated with increasing signal-to-noise ratio (or amplitude). For its part, MO99 gives a constant overestimate by a factor of about three for all S/N ratios. We note that Equation 1c is obtained by averaging the observed time. A change in the zero-point of time will introduce a constant factor to that equation that could correct for the observed difference. While investigating further the reasons behind these differences could be of interest, we stick to our main goal here, which is to calibrate our method to estimate errors accurately. Based on the tests presented above, we thus validated our method to compute uncertainties for the amplitude and frequency, and we implemented a normal-

ized method (MO99 formula divided by a constant value 3) to estimate phase uncertainties.

3. KEPLER PHOTOMETRY

In this work, all data were obtained from the *Kepler* space telescope during its initial survey phase. We only analyzed short-cadence (58.85 s) light curves distributed through the MAST² website. This exposure allows us to detect rapid oscillations in compact pulsating stars (see, e.g., [Charpinet et al. 2011](#)). KIC 2438324 was continuously observed from Q6.1 to Q17.2, for a total duration of 35 months. KIC 11179657 was observed in several segments, Q2.3, Q5.1-Q7.3, Q9.1-Q11.3, Q13.1-Q15.3 and Q17.1-Q17.2, because this star fell on the nonfunctional CCD Module 3 every four quarters, due to the onboard photometer being rolled by 90 degrees every ~ 93 days. This rotation of the instrument may induce fluctuations of the contamination factor of some targets, as images of these stars relocate onto different CCD modules. The initial one-month run Q2.3 was not further considered, due to its long disconnection with the main part

² The Mikulski Archive for Space Telescopes:
<http://archive.stsci.edu/kepler/>

Table 1. Contamination values per quarter for KIC 2438324 and KIC 11179657 during the main campaign.

| Quarter | KIC 2438324 | KIC 11179657 |
|---------|-------------|--------------|
| 5 | - | 0.0001 |
| 6 | 0.046 | 0 |
| 7 | 0.414 | 0 |
| 8 | 0.007 | - |
| 9 | 0.031 | 0.0002 |
| 10 | 0.047 | 0 |
| 11 | 0.416 | 0 |
| 12 | 0.007 | - |
| 13 | 0.032 | 0.0001 |
| 14 | 0.046 | 0 |
| 15 | 0.418 | 0 |
| 16 | 0.007 | - |
| 17 | 0.032 | 0 |

of the *Kepler* observations. Table 1 lists the contamination values reported at different quarters for KIC 2438324 and KIC 11179657. KIC 2438324 lightcurve was contaminated by nearby stars with a factor varying from 0.007 to 0.418. In contrast, KIC 11179657 lightcurve has almost never suffered pollution from the light of nearby stars, with a maximum factor of 0.0002.

In the following, both raw and corrected light curves are analyzed. These were produced through the standard Ke-

pler Science Processing Pipeline provided by Jenkins et al. (2010). As in Paper I, we performed additional data detrending and 3σ -clipping to remove residual drifts and data point outliers. After these operations, the raw and corrected light curves for KIC 11179657 consist of 1,413,308 and 1,399,858 points, with duty cycles of 91.6% and 90.7%, respectively, over a period of ~ 2.88 years. For KIC 2438324, the light curves contain 1,227,891 and 1,235,149 measurements for the corrected and raw flux, corresponding to duty cycles of 72.9% and 73.3%, respectively, over ~ 3.14 years. The two light curves are shown in their entirety on the top panels of Figure 2. A clear feature related to KIC 2438324 is that light variations in the corrected flux are significantly higher than that of the raw flux when the contamination factor is large (see Table 1). Parts of the light curves are expanded in bottom panels where the brightness variations from the binary reflection effect dominate over the pulsations. The latter are however clearly seen in the Lomb-Scargle Periodograms (LSP; Lomb 1976; Scargle 1982) represented in Figure 3. The two stars show very similar LSPs with oscillations mostly in the low-frequency *g*-mode domain between 100 and 400 μHz , and few low-amplitude modes in the 400 – 600 μHz range. However, the noise level for KIC 11179657 is much lower than that of KIC 2438324, although their main frequencies have very similar amplitudes, ~ 2 ppt. We note that the amplitudes of oscillations in KIC 2438324 differ in the two types of fluxes, mainly due to contaminating light from the nearby star.

Table 2. List of frequencies detected in KIC 2438324.

| Id. | Frequency (μHz) | σ_f (μHz) | Period (s) | σ_p (s) | Amplitude (ppt) | σ_A (ppt) | S/N | Modulation ^d |
|-------------------|---------------------------------|----------------------------------|---------------|-------------------|--------------------|---------------------|-------|-------------------------|
| f_{orb} | 29.044187 | 0.000018 | 34430.297397 | 0.021593 | 13.383 | 0.0040 | 333.1 | AM |
| $2f_{\text{orb}}$ | 58.088335 | 0.000113 | 17215.160472 | 0.033617 | 2.149 | 0.0040 | 53.5 | AM |
| f_{12} | 130.864047 | 0.000442 | 7641.518249 | 0.025805 | 0.545 | 0.040 | 13.7 | AM |
| f_{01} | 216.283646 | 0.000129 | 4623.558085 | 0.002761 | 1.837 | 0.039 | 47.0 | AFM |
| f_{10} | 216.891302 | 0.000346 | 4610.604431 | 0.007357 | 0.685 | 0.039 | 17.5 | AFM |
| f_{09} | 217.487634 | 0.000342 | 4597.962562 | 0.007240 | 0.692 | 0.039 | 17.7 | AFM |
| f_{18} | 229.002081 | 0.000656 | 4366.772541 | 0.012516 | 0.360 | 0.039 | 9.2 | ... |
| f_{06} | 229.606249 | 0.000296 | 4355.282166 | 0.005623 | 0.796 | 0.039 | 20.5 | AM |
| f_{03} | 241.516688 | 0.000223 | 4140.500628 | 0.003821 | 1.058 | 0.039 | 27.2 | AM |
| f_{14} | 273.479046 | 0.000451 | 3656.587279 | 0.006035 | 0.519 | 0.039 | 13.4 | AM |
| f_{16} | 290.442213 | 0.000520 | 3443.025692 | 0.006159 | 0.450 | 0.039 | 11.7 | ... |

Table 2 continued

Table 2 (continued)

| Id. | Frequency (μHz) | σ_f (μHz) | Period (s) | σ_P (s) | Amplitude (ppt) | σ_A (ppt) | S/N | Modulation ^a |
|----------|---------------------------------|----------------------------------|---------------|-------------------|--------------------|---------------------|------|-------------------------|
| f_{02} | 291.709724 | 0.000216 | 3428.065358 | 0.002535 | 1.083 | 0.039 | 28.1 | AM |
| f_{05} | 316.834658 | 0.000275 | 3156.220361 | 0.002738 | 0.848 | 0.038 | 22.1 | AM |
| f_{22} | 317.483152 | 0.001047 | 3149.773437 | 0.010388 | 0.223 | 0.038 | 5.8 | ... |
| f_{15} | 318.110788 | 0.000456 | 3143.558902 | 0.004508 | 0.511 | 0.038 | 13.3 | AM |
| f_{20} | 339.332074 | 0.000881 | 2946.965748 | 0.007654 | 0.264 | 0.038 | 6.9 | ... |
| f_{07} | 342.428859 | 0.000304 | 2920.314614 | 0.002597 | 0.762 | 0.038 | 19.9 | AFM |
| f_{13} | 343.691933 | 0.000443 | 2909.582399 | 0.003751 | 0.524 | 0.038 | 13.7 | AFM |
| f_{08} | 372.630047 | 0.000318 | 2683.626853 | 0.002290 | 0.730 | 0.038 | 19.1 | AFM |
| f_{04} | 373.893293 | 0.000243 | 2674.559880 | 0.001735 | 0.957 | 0.038 | 25.0 | AFM |
| f_{11} | 404.773515 | 0.000412 | 2470.517370 | 0.002513 | 0.563 | 0.038 | 14.7 | AM |
| f_{17} | 406.037063 | 0.000515 | 2462.829359 | 0.003122 | 0.450 | 0.038 | 11.8 | AM |
| f_{19} | 419.376109 | 0.000685 | 2384.494441 | 0.003896 | 0.337 | 0.038 | 8.9 | ... |
| f_{21} | 470.044374 | 0.000960 | 2127.458713 | 0.004344 | 0.240 | 0.038 | 6.3 | ... |

^aNote: Amplitude (AM) and amplitude/frequency (AFM) modulation provided for that frequency. See text for details.

Table 3. List of frequencies detected in KIC 1117657.

| Id. | Frequency (μHz) | σ_f (μHz) | Period (s) | σ_P (s) | Amplitude (ppt) | σ_A (ppt) | S/N | Modulation ^a |
|-------------------|---------------------------------|----------------------------------|---------------|-------------------|--------------------|---------------------|-------|-------------------------|
| f_{orb} | 29.341850 | 0.000011 | 34081.013757 | 0.012466 | 9.211 | 0.0018 | 518.1 | AM |
| $2f_{\text{orb}}$ | 58.683671 | 0.000149 | 17040.515462 | 0.043206 | 0.661 | 0.0018 | 37.4 | AM |
| f_{20} | 119.619242 | 0.000582 | 8359.859033 | 0.040645 | 0.168 | 0.018 | 9.6 | ... |
| f_{07} | 122.555274 | 0.000212 | 8159.583591 | 0.014084 | 0.463 | 0.018 | 26.3 | ... |
| f_{21} | 146.298704 | 0.000588 | 6835.330534 | 0.027491 | 0.166 | 0.018 | 9.5 | ... |
| f_{32} | 151.816132 | 0.000857 | 6586.915297 | 0.037182 | 0.114 | 0.018 | 6.5 | ... |
| f_{22} | 163.867034 | 0.000618 | 6102.508697 | 0.023010 | 0.157 | 0.017 | 9.0 | ... |
| f_{25} | 185.725763 | 0.000662 | 5384.282638 | 0.019193 | 0.147 | 0.017 | 8.4 | ... |
| f_{01} | 186.484826 | 0.000058 | 5362.366591 | 0.001682 | 1.659 | 0.017 | 95.1 | AM |
| f_{11} | 194.925628 | 0.000291 | 5130.161738 | 0.007651 | 0.333 | 0.017 | 19.1 | AFM |
| f_{02} | 195.724900 | 0.000060 | 5109.211964 | 0.001574 | 1.608 | 0.017 | 92.2 | AFM |
| f_{30} | 196.505979 | 0.000765 | 5088.903694 | 0.019817 | 0.127 | 0.017 | 7.3 | ... |
| f_{15} | 206.580304 | 0.000424 | 4840.732551 | 0.009943 | 0.228 | 0.017 | 13.1 | ... |
| f_{31} | 207.379992 | 0.000826 | 4822.065951 | 0.019216 | 0.117 | 0.017 | 6.7 | ... |
| f_{24} | 218.282801 | 0.000657 | 4581.212980 | 0.013785 | 0.147 | 0.017 | 8.5 | ... |
| f_{13} | 231.820585 | 0.000373 | 4313.680766 | 0.006944 | 0.258 | 0.017 | 14.9 | ... |
| f_{34} | 233.913634 | 0.001002 | 4275.082137 | 0.018305 | 0.096 | 0.017 | 5.6 | ... |
| f_{29} | 253.113331 | 0.000738 | 3950.799422 | 0.011517 | 0.130 | 0.017 | 7.5 | ... |

Table 3 continued

Table 3 (*continued*)

| Id. | Frequency (μHz) | σ_f (μHz) | Period (s) | σ_p (s) | Amplitude (ppt) | σ_A (ppt) | S/N | Modulation ^a |
|----------|---------------------------------|----------------------------------|---------------|-------------------|--------------------|---------------------|------|-------------------------|
| f_{23} | 260.392034 | 0.000644 | 3840.363259 | 0.009503 | 0.149 | 0.017 | 8.6 | ... |
| f_{26} | 261.632760 | 0.000704 | 3822.151326 | 0.010288 | 0.136 | 0.017 | 7.9 | ... |
| f_{28} | 263.969777 | 0.000730 | 3788.312483 | 0.010480 | 0.132 | 0.017 | 7.6 | ... |
| f_{18} | 265.556190 | 0.000473 | 3765.681381 | 0.006706 | 0.203 | 0.017 | 11.8 | ... |
| f_{14} | 269.269969 | 0.000417 | 3713.744995 | 0.005757 | 0.230 | 0.017 | 13.3 | ... |
| f_{09} | 283.831342 | 0.000226 | 3523.219084 | 0.002802 | 0.426 | 0.017 | 24.6 | AFM |
| f_{04} | 284.629468 | 0.000095 | 3513.339662 | 0.001169 | 1.014 | 0.017 | 58.7 | AFM |
| f_{08} | 285.409755 | 0.000210 | 3503.734486 | 0.002581 | 0.457 | 0.017 | 26.4 | AFM |
| f_{16} | 295.574098 | 0.000434 | 3383.246395 | 0.004964 | 0.221 | 0.017 | 12.8 | ... |
| f_{12} | 307.855429 | 0.000330 | 3248.277947 | 0.003484 | 0.290 | 0.017 | 16.8 | AFM |
| f_{06} | 308.657235 | 0.000175 | 3239.839820 | 0.001838 | 0.547 | 0.017 | 31.8 | AFM |
| f_{19} | 309.438786 | 0.000549 | 3231.656942 | 0.005736 | 0.174 | 0.017 | 10.1 | ... |
| f_{03} | 337.173926 | 0.000065 | 2965.828388 | 0.000575 | 1.456 | 0.017 | 85.0 | AM |
| f_{17} | 337.954922 | 0.000441 | 2958.974514 | 0.003863 | 0.216 | 0.017 | 12.6 | ... |
| f_{05} | 338.298358 | 0.000162 | 2955.970598 | 0.001418 | 0.587 | 0.017 | 34.3 | AM |
| f_{33} | 368.217265 | 0.000878 | 2715.787918 | 0.006474 | 0.108 | 0.017 | 6.3 | ... |
| f_{10} | 369.030407 | 0.000263 | 2709.803799 | 0.001930 | 0.361 | 0.017 | 21.2 | AM |
| f_{27} | 558.210809 | 0.000692 | 1791.437901 | 0.002220 | 0.136 | 0.017 | 8.0 | ... |

^aNote: Amplitude (AM) and amplitude/frequency (AFM) modulation provided for that frequency. See text for details.

Frequency extraction follows the same procedure as in Paper I, which is based on a standard prewhitening and non-linear least-squares fitting approach (Deeming 1975). We provide in Table 2 and 3 the lists of detected peaks for KIC 2438324 and KIC 11179657 respectively along with their fitted attributes : frequency (in μHz ; and period in seconds), amplitude (in ppt, i.e., parts per thousand) relative to the mean brightness of the star, and signal-to-noise ratio (S/N) of the detection. Each attribute has an associated error : σ_f , σ_p , and σ_A . The “ID” column uniquely identifies a detected frequency with a sequence number that indicates its rank by order of decreasing amplitude. The “Modulation” column indicates if amplitude only (AM: for characterization of systematic modulations) or amplitude/frequency modulations (AFM: in representative rotational multiplets) are presented here for a given frequency. These modes are further discussed in the following sections.

Table 2 lists 22 detected frequencies in KIC 2438324 associated to stellar oscillations and two additional low-frequency peaks of orbital nature. All of them are above an adopted threshold of $5.6 \times$ the noise level (5.6σ as tested in Zong et al. 2016a). There are 16 frequencies attributed to components of two triplets near 217 and 317 μHz , and five doublets near 229, 291, 342, 372 and 406 μHz . One compo-

nent, f_{16} , of the doublet near 290 μHz falls close to ten times the orbit frequency, $f_{\text{orb}} \sim 29 \mu\text{Hz}$. We note that all frequencies are found in the 100–500 μHz range. For KIC 11179657 (Table 3), we detected 33 independent frequencies above 5.6σ , all attributed to oscillations. We identify three triplets near 195, 284 and 307 μHz , four doublets near 185, 206, 337 and 368 μHz , and a possible quintuplet near 260 μHz with two missing components. Table 3 also contains a frequency, f_{32} , which is close to the difference of f_{05} and f_{01} . We further note that two weak peaks (of $S/N \sim 5$; i.e., not provided in Table 3) are seen at 336.37 μHz and 262.88 μHz . These could be additional components belonging to the doublet near 337 μHz and the 260 μHz quintuplet, respectively. In addition to the oscillations, we also detected a binary signal, f_{orb} , at a frequency of 29.341850 μHz and its first harmonic $2f_{\text{orb}}$. Like for KIC 2438324, most of the frequencies of KIC 11179657 are found in the 100–400 μHz frequency range, except the frequency f_{27} at 558.2 μHz .

4. MODULATION PATTERNS

Following the same strategy as in Paper I to analyze amplitude and frequency modulations in these two stars, we focus on frequencies of highest amplitudes, in particular those being components of rotational multiplets. We note that, for

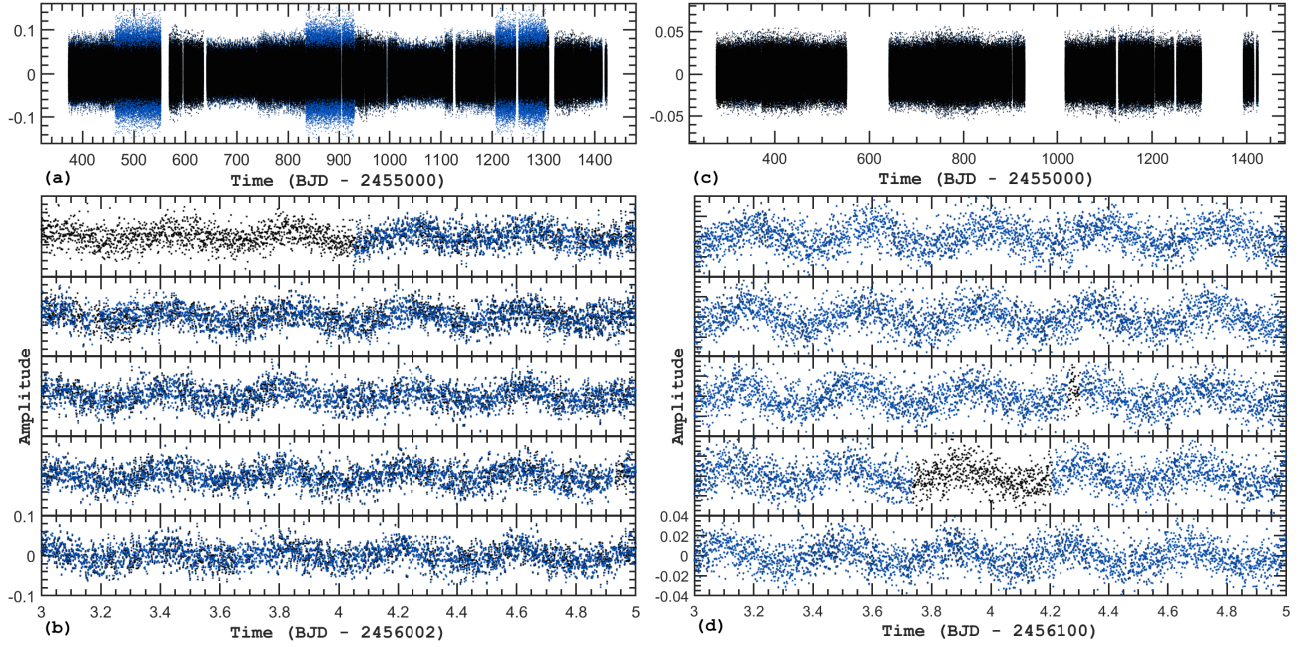


Figure 2. Assembled light curves (amplitude is the residual flux relative to the mean brightness of the star vs. time in relative Barycentric Julian Date) of KIC 2438324 (a) and KIC 11179657 (c) from the *Kepler* observations. Expanded views show ten days of the light curves by slices of two days for KIC 2438324 (b) and KIC 11179657 (d). Raw and corrected fluxes are in black and dark blue, respectively. These colors are also adopted for the following figures 3 to 7.

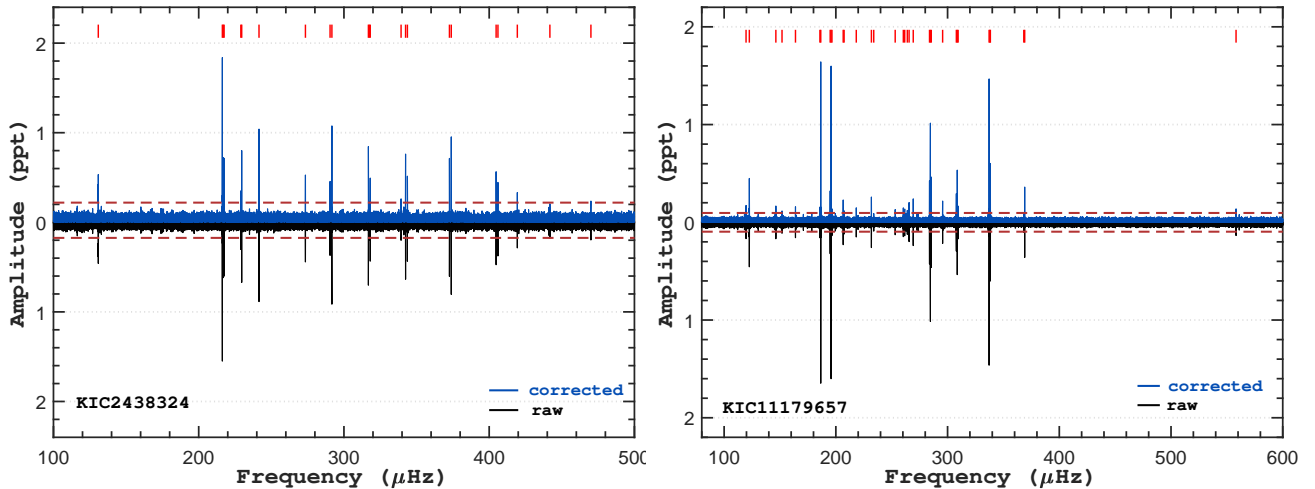


Figure 3. Parts of LSP of the *Kepler* photometry collected on KIC 2438324 (right) and KIC 11179657 (left), covering the frequency range where the pulsation signals are found. The vertical segments locate the position of the detected signals. The dashed horizontal lines are the 5.6σ threshold of the local noise. A distinct feature of amplitude difference is clearly seen between the raw (upside-down) and corrected LSP of KIC 2438324 but not KIC 11179657.

both stars, there are relatively few frequencies compared to KIC 3527751 discussed in Paper I. Contrary to paper I, we do not provide sliding LS-Periodograms (sLSP) due to two specific limitations: (1) In general, we find that most frequencies are close to stability and do not show obvious variations in these diagrams, as they are not sensitive enough. (2) They are of limited use to precisely measure modulation patterns for comparison between raw and corrected fluxes (the main

objective of the present analysis). In the following, we therefore only present the modulations obtained by prewhitening the frequencies in various parts of the light curve. The 35-month light curve of KIC 2438324 was divided into a series of adjacent pieces using a time step of about 10 d and a filtering window of width 180 d. Each part was analyzed using the same prewhitening technique applied to the whole light curve. This provided 95 measurements for all frequencies

with amplitudes above ~ 0.7 ppt. More details on how to obtain measurements from each light-curve segment can be found in Section 4.2 of Paper I. For KIC 11179657, the light curve was divided into pieces of time step ~ 15 d and window width of 120 d. The difference of time step (10 d vs 15 d) does not change the general patterns of the amplitude and frequency modulations, but using the longer time step was necessary to reduce computation time. The time window size of 120 d was chosen to ensure sufficient resolution in frequency and to minimize contamination from side-band frequencies associated to the orbital signal with very large amplitude that suffers instrumental amplitude modulations. Since this star experienced two long interruptions of its monitoring, a few measurements were discarded when they were very close to large interval gaps. We finally obtained 45 measurements for the frequencies of amplitude above ~ 0.3 ppt.

4.1. Representative frequencies in KIC 2438324

In the following, we do not provide AMs and FMs for frequencies with S/N lower than ~ 12 , due to their small number of exploitable measurements. We end up with 16 frequencies that contain more than 50 measurements each. In this section, we focus on AMs and FMs occurring in one triplet and two doublets as representative modes to illustrate the differences encountered with raw and corrected photometric data. For the other modes, the uncovered patterns will be discussed in Section 5.

Figure 4 shows the AMs and FMs detected in the triplet components near $216.9 \mu\text{Hz}$. The LSP of the full light curve shows rather simple peak structures suggesting that the three components experience only weak modulations. This is confirmed by the precise measurements of the modulation patterns presented in the middle and right panels. The retrograde ($m = -1$) component of the triplet displays frequency variations within $\sim \pm 2$ nano Hz, i.e., comparable to the uncertainties. The other two components show larger FMs of $\sim \pm 10$ nano Hz. Besides, during most of the observing run, the FMs appear to be somewhat antiphased between the $m = 0$ and $m = -1$ components. Comparing now the two data reduction levels (raw vs corrected flux), we find that FMs of the three components are very similar. However, the two different types of AM patterns show some differences. For instance, the retrograde mode evolves in apparent antiphase over most of the observations. Despite these differences, we find that these AMs show very similar modulation patterns in each type of flux, overall, which is further illustrated in Figure 8.

Figure 5 illustrates the AMs and FMs disclosed in the components forming two doublets near 343 and $373 \mu\text{Hz}$, respectively. The structures in the LSP near these two doublets have, again, relatively simple forms, similar to that of the $216.9 \mu\text{Hz}$ triplet. The two ($m = \pm 1$) components form-

ing the $343 \mu\text{Hz}$ doublet clearly exhibit some anti-correlation during most of the observing run, with almost the same values extracted from both types of fluxes. For the FMs occurring in the $373 \mu\text{Hz}$ doublet, as measured from the two types of fluxes, the pulse-shape frequency variations only look anti-phased when the ($m = +1$) component reaches its frequency maximum, but with a phase delay of one month. We find that the four frequency variations are within a range of ± 10 nano Hz. Concerning measured AMs, they appear clearly different in the raw and corrected fluxes, respectively. However, despite these differences, all of them seem to follow similar patterns. We note that the amplitude uncertainty of the $344 \mu\text{Hz}$ component is relative large compared to the other three modes.

4.2. Representative frequencies in KIC 11179657

Similar to KIC 2438324, AMs and FMs are provided for one triplet and two doublets as representative frequencies observed in KIC 11179657. In this case, we measured AMs and FMs for modes with S/N values down to about 20, a bit higher than for KIC 2438324. This establishes 11 modes with measured modulations out of 34 detected frequencies. This higher S/N limit is chosen because the light curves run across two large interval gaps. Details on these 11 frequencies with precise AMs and FMs are presented in Section 5.

Figure 6 shows the AMs and FMs disclosed in the components belonging to the triplet near $284.6 \mu\text{Hz}$. The nearly equidistant triplet reveals broadened structures in the LSP for each component, due to aliasing introduced by the large gaps in the light curves. A noticeable feature is that both AMs and FMs show almost the same patterns whatever the flux calibration used. The $m = \pm 1$ components show regular frequency variations evolving in antiphase for some events. The quasi-periodic FMs can be roughly estimated to be on a timescale of one year, with a magnitude of ± 10 nano Hz. In contrast, the central ($m = 0$) component exhibits a less obvious FM, with a magnitude of ± 4 nano Hz. The AMs happening in this triplet reveal relatively simple patterns, e.g., the central component following a roughly linear increase in amplitude during the whole observation run. We also note that the $m = -1$ and $m = 0$ components have very similar AMs during the last observation segment. However, in the first segment, the similar AMs are found between the $m = +1$ and $m = 0$ components.

Figure 7 shows the AMs and FMs obtained for the components forming two doublets near 196 and $308 \mu\text{Hz}$, respectively. These doublets, similar to the triplet previously described, show no difference in the measurements of amplitude and frequency modulations from the raw and corrected fluxes. The $196 \mu\text{Hz}$ doublet has regular frequency variations, which first evolve in phase (the first segment), then gradually switch to antiphase (the last segment) between the

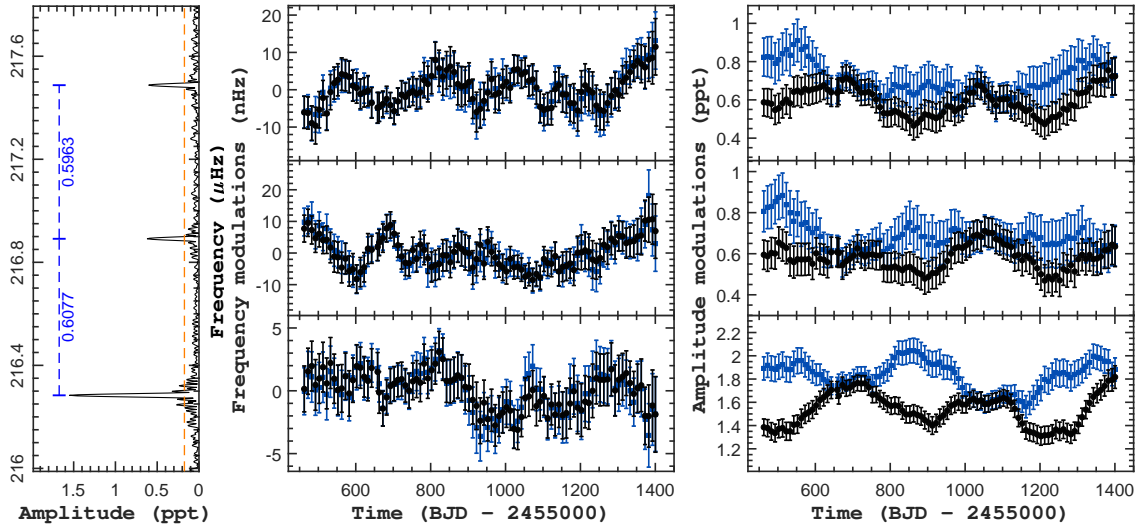


Figure 4. Amplitude (AM) and frequency modulations (FM) of the triplet components near $217\ \mu\text{Hz}$ in KIC 2438324. *Left panel:* the LSP shows nearly equidistant structures whose frequency spacing values are given in the text. The dashed line is our typical detection limit of 5.6σ above local median noise. The corresponding FMs and AMs of each component, measured from two different correction levels of the photometric data, are presented in the *middle* and *right* panels, respectively. Note that the FMs are shifted to their averaged values.

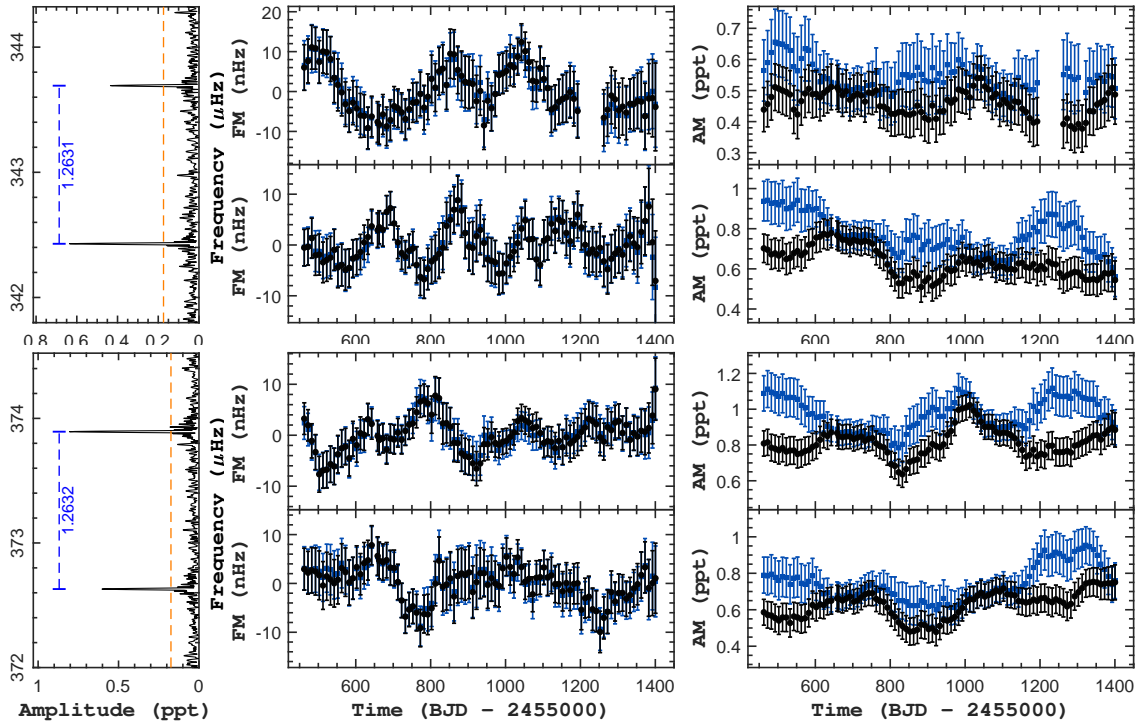


Figure 5. Same to Figure 4 but for an example of two doublets near 343 and $373\ \mu\text{Hz}$ in KIC 2438324 (from top to bottom panels), respectively.

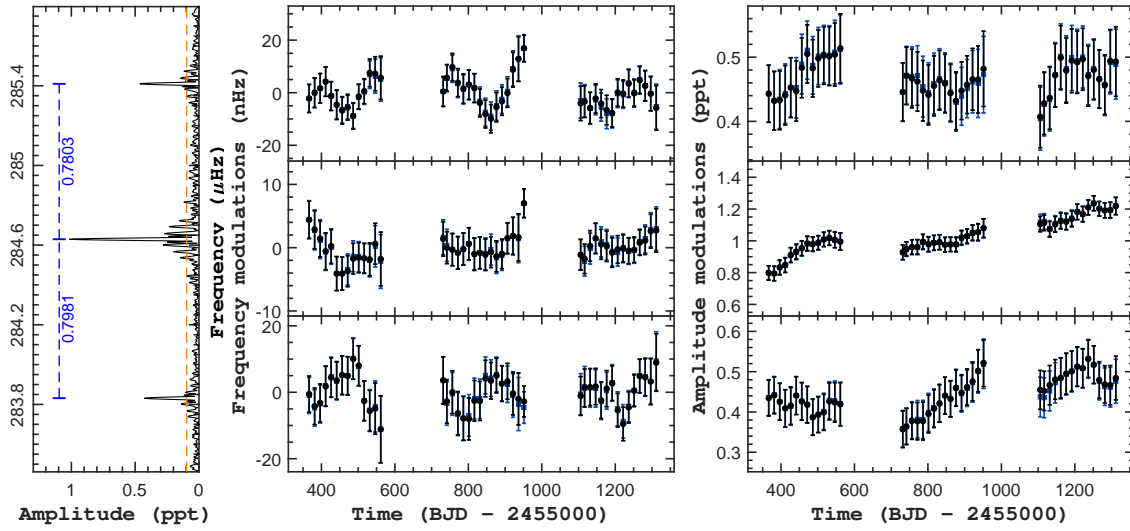


Figure 6. Same to Figure 4 but for an example of triplet near $284.6 \mu\text{Hz}$ in KIC 11179657. Note that, at this scale, the two different measurements are very close to each others both in amplitude and frequency.

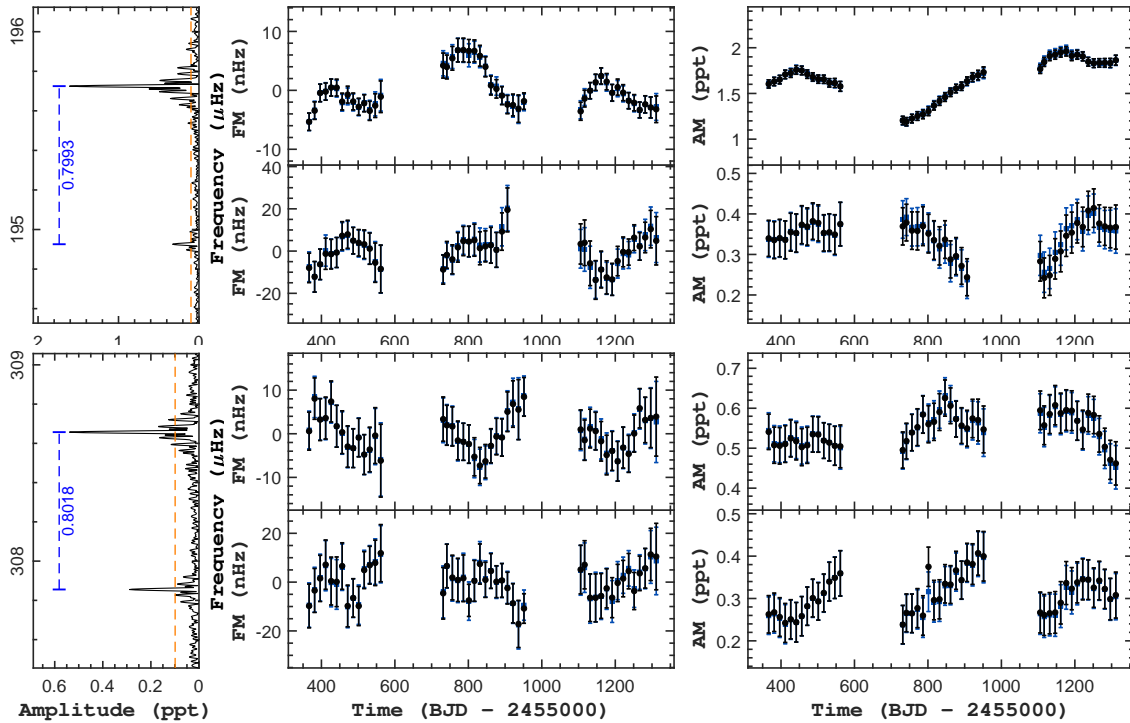


Figure 7. Same to Figure 4 but for examples of two triplets near 196 and $308 \mu\text{Hz}$ in KIC 11179657 (from top to bottom panels), respectively. Note that both triplets have one weak side component whose AM is not provided due to its small amplitude.

two components. The FMs measured in the $308\ \mu\text{Hz}$ doublet show the opposite, by first evolving somewhat in antiphase, then gradually becoming in phase, if we roughly estimate the modulation patterns. All these four components are measured with relatively small FMs, typically within a range of ± 10 nano Hz. A closer look at the AMs of these components suggests possibly regular modulation patterns. The $196\ \mu\text{Hz}$ doublet possibly exhibits anti-correlation between its two components. However, the $308\ \mu\text{Hz}$ doublet does not show clear correlations in the variations occurring between the two components.

5. COMPARISON WITH AN ORBITAL SIGNAL

As described in the above section, the representative frequencies may have very similar modulation patterns in their amplitudes, which intuitively suggests instrumental effects from the satellite itself. To carefully check for such effects, reliable references should be used as calibrators for the amplitude. Binary signals, such as observed in KIC 2438324, can be good candidates for such references, due to their usually high amplitudes (enough precision) and several harmonics (systematic variation) showing up in the LSP. The orbital period is normally stable in a sdB+dM binary system over a time baseline of ~ 3 yr (see, e.g., Lee et al. 2009). It is therefore natural to use this binary signal to gauge the variations observed in modes with AMs and FMs.

Figure 8 shows the comparison of AMs measured in the orbital frequency (f_{orb}) and its first harmonic ($2f_{\text{orb}}$) with AMs obtained for 13 independent pulsation frequencies of KIC 2438324. This clearly establishes that f_{orb} (and its harmonics) are subject to almost exactly the same modulation patterns, both in the raw and corrected flux data sets. Moreover, in general, the AMs of the independent pulsation frequencies are very similar to that of f_{orb} , since all measurements are consistent with the AM of f_{orb} within the uncertainties. The AMs of f_{orb} are measured with peak-to-peak variations of $\sim 10\%$ and $\sim 5\%$ using the raw and corrected fluxes, respectively. These values also correspond to the magnitude of the variations observed in the 13 independent modes. We also note that the modulation patterns are different, when comparing raw and corrected fluxes, both in terms of amplitudes and phases of the effect. Another observation worth noting is that the corrected AMs of the independent frequencies follow less closely to that of f_{orb} than the raw AMs (as revealed by a careful comparison of the two panels of Figure 8).

Figure 9 compares AMs of f_{orb} and its first harmonic with the other three frequencies, f_{02} , f_{12} and f_{15} , with available measurements in KIC 2438324. We find that the modulation patterns are significantly different in these cases, in particular for f_{12} whose AM exhibits a large $\sim 50\%$ peak-to-peak variation. This frequency seems to experience three local max-

ima and minima (with two missing measurements due to the amplitude becoming too low). Moreover, we note that the two other frequencies, f_{02} and f_{15} , have AMs that are not following the general trend of f_{orb} in general, although there is some overlap between the modulations.

Figure 10 shows the comparison of AMs between the orbital frequency, f_{orb} , and 11 independent frequencies of KIC 11179657. We only provide the raw AM patterns for these frequencies considering that this star is only slightly contaminated (also see Figure 6 and 7). In contrast with what we observe for KIC 2438324, we find that f_{03} presents a very similar modulation pattern compared to f_{orb} over the entire observation run. However, if we compare the modulation patterns in each observational segment, then almost all frequencies show similar AM patterns in at least one segment, such as f_{02} (in the first part) and f_{05} (in the middle and last parts), considering the uncertainties of the measurements. In addition, we find that the two independent frequencies may have similar AMs at some observational segment. For instance, AM patterns of f_{09} and f_{12} are found to be somewhat similar to the AM of f_{02} in the middle observation segment. Whether this is a coincidence or due to calibration issues needs further investigation.

6. DISCUSSION

The results presented in this paper are the continuation of our project to analyze AMs and FMs in compact pulsators by exploiting the full data sets available from *Kepler*. A natural explanation for such phenomena is the weak nonlinear interaction between resonant modes, which can produce diverse modulation patterns (Buchler et al. 1995, 1997). However, our detailed studies of KIC 2438324 and KIC 11179657 lead to the discovery of systematic AMs for several of the independent pulsation modes identified in these two stars. This behavior is different from previous modulations characterized in several compact pulsating stars (Zong et al. 2016a,b, Paper I). It is plausible that this kind of AMs may be induced by instrumental effects onboard or by the data reduction pipeline. This finding adds further complexity to the goal of precisely measuring the intrinsic amplitudes of oscillations or other signals (e.g., transits of planets).

6.1. Comparison of frequency content with previous results

KIC 2438324 and KIC 11179657 show a much lower number of frequencies than that detected in KIC 3527751 (Paper I), i.e., a few tens compared to more than two hundred. In both stars, the frequency contents are similar with modes detected in the $[100, 600]\ \mu\text{Hz}$ range. In KIC 2438324, most of the frequencies already detected in Pablo et al. (2011) are recovered, except one low-amplitude (suspected) frequency at $405.45\ \mu\text{Hz}$ although we have analyzed a light curve more than six times longer than theirs. From our analysis, we only

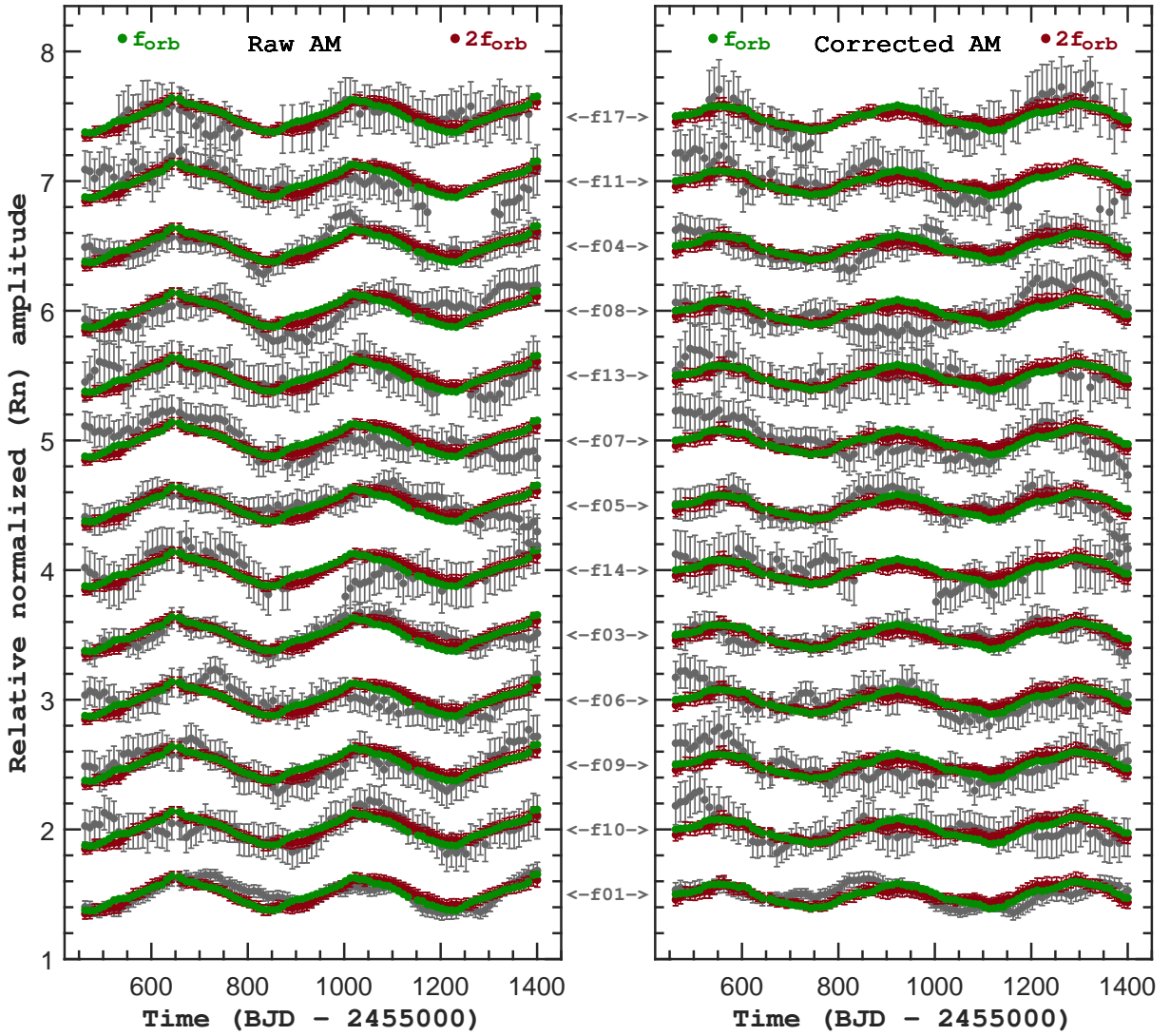


Figure 8. AM comparison of 13 independent frequencies with the orbital frequencies in the sdB star KIC 2438324. *Left panel* shows AMs measured from the raw flux and *right* from the corrected flux. Each of these frequencies are normalized by their averaged amplitudes and shifted to the values where the legends indicate. Note that the errors for the orbital frequency f_{orb} are smaller than the symbol itself.

have four additional low-amplitude frequencies not seen in Pablo et al. (2011), which complete the triplet near $319 \mu\text{Hz}$ and the independent frequency around $290 \mu\text{Hz}$ that is now a doublet. Compared to Pablo et al. (2012), we have recovered all their frequencies from our 5.6σ level, except one at $262.8 \mu\text{Hz}$ which is nonetheless obtained if we allow $S/N \sim 5.1$ to be a trustworthy detection. As the noise level decreases, we find eight additional weak frequencies, which complete the former doublet at $195 \mu\text{Hz}$ to make it a triplet, and two former independent frequencies near 206 and $369 \mu\text{Hz}$ which are now doublets.

Both stars show a rich set of multiplets interpreted as rotational splittings and relatively few independent frequencies. These may prove to be good candidates for further seismic modelling (see, e.g., Charpinet et al. 2005). At present, there is no detailed seismic result obtained for sdB pulsators with

the full *Kepler* photometry yet. Considering their similar frequency contents and orbital periods, it will be interesting to compare their internal structural and dynamical properties through the technique of asteroseismology (see, e.g., Charpinet et al. 2008).

6.2. Modulation patterns

All representative pulsation modes illustrated in this paper are discovered with variations in amplitude and frequency. Considering that our evaluations of the uncertainties are proven to be robust (Section 2), we believe that the values determined for the amplitudes and frequencies are highly confident. Besides, AMs and FMs from the two different flux calibrations (raw and corrected) can serve as a way to double check the determined values. Our results suggest that the frequency modulations show consistent patterns, when

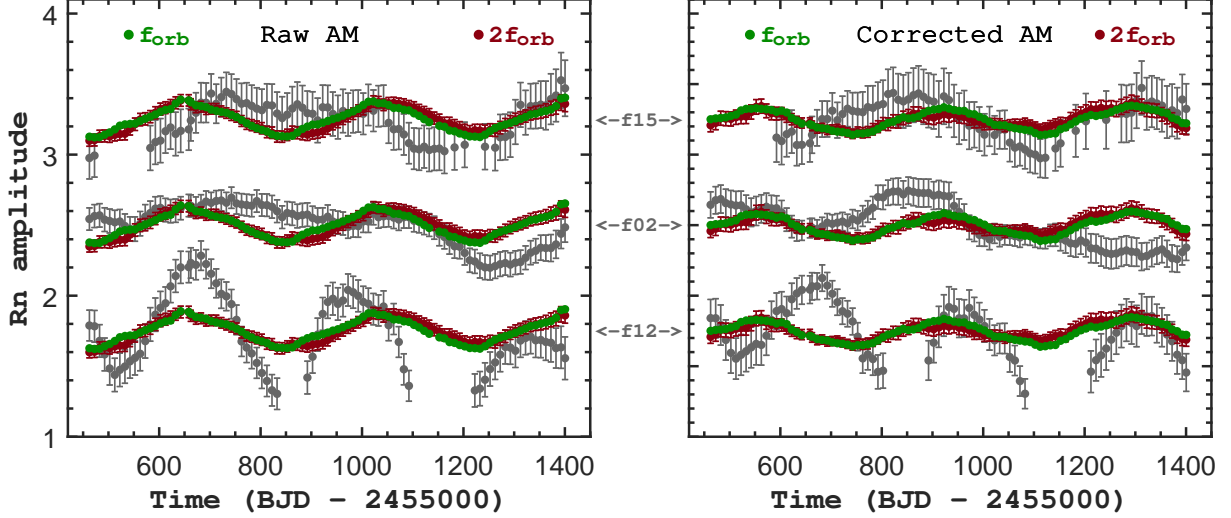


Figure 9. Same to Figure 8 but for another three independent frequencies in KIC 2438324. Note that these AMs are significantly different to those in Figure 8

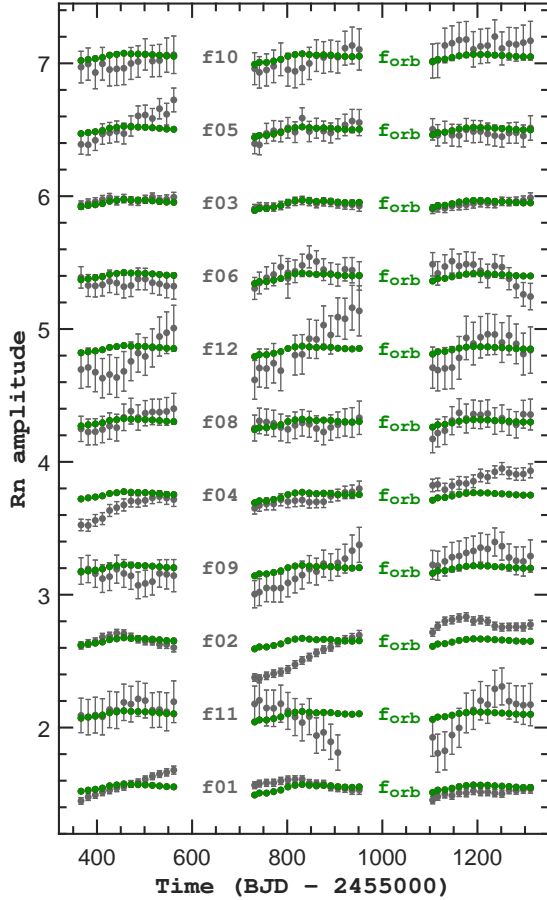


Figure 10. AM comparison of 11 independent frequencies with the orbital frequency in the sdB star KIC 11179657. Each of these frequencies are normalized by their averaged amplitudes and shifted to the values where the legends indicate. Note that the errors for the orbital frequency f_{orb} are smaller than the symbol itself.

measured alternatively from the raw and corrected fluxes, for both stars (see Figure 4-7). However, the correction of the flux introduces a significant difference in AMs patterns when the fraction of contaminating light coming from nearby background or foreground objects is large. For instance, in KIC 2438324 we not only observe that the values of peak-to-peak variation are different, but also that the phase of the AMs shifts between raw and corrected data for the same frequency. The corrected AMs also follow that of f_{orb} less closely than the raw AMs. All these observations suggest that the correction of raw flux brings an extra signal to AMs, as the contamination factor increases. FMs remain unaffected by this effect because we extract the highest peaks even if the AMs induce symmetric (weak) side-bands around those peaks in LSP.

We recall that nonlinear resonant interactions between three modes forming a triplet can produce various AMs and FMs (Buchler et al. 1995, 1997; Goupil et al. 1998) featuring stable, periodic, or irregular modulation pattern. All the representative frequencies discussed previously satisfy this triplet resonance condition (doublets are incomplete triplets with an undetected component). Considering the uncertainties, the detected AMs and FMs in the representative frequencies might be associated with the intermediate regimes of the triplet resonance (see such examples in Zong et al. 2016a,b). We clearly see quasi-periodic FMs occurring on timescales of several months to well over a year, as shown in Figure 11, which is comparable to the timescale that corresponds to the frequency mismatch of $\sim 0.01 \mu\text{Hz}$ and $\sim 0.02 \mu\text{Hz}$ in the triplets $217 \mu\text{Hz}$ (KIC 2438324) and $284 \mu\text{Hz}$ (KIC 11179657), respectively. From this figure, we clearly see various configurations, which indicates that their modulation patterns are indeed different (as roughly displayed in Figure 4-7). Nevertheless, as nonlinear resonant coupling

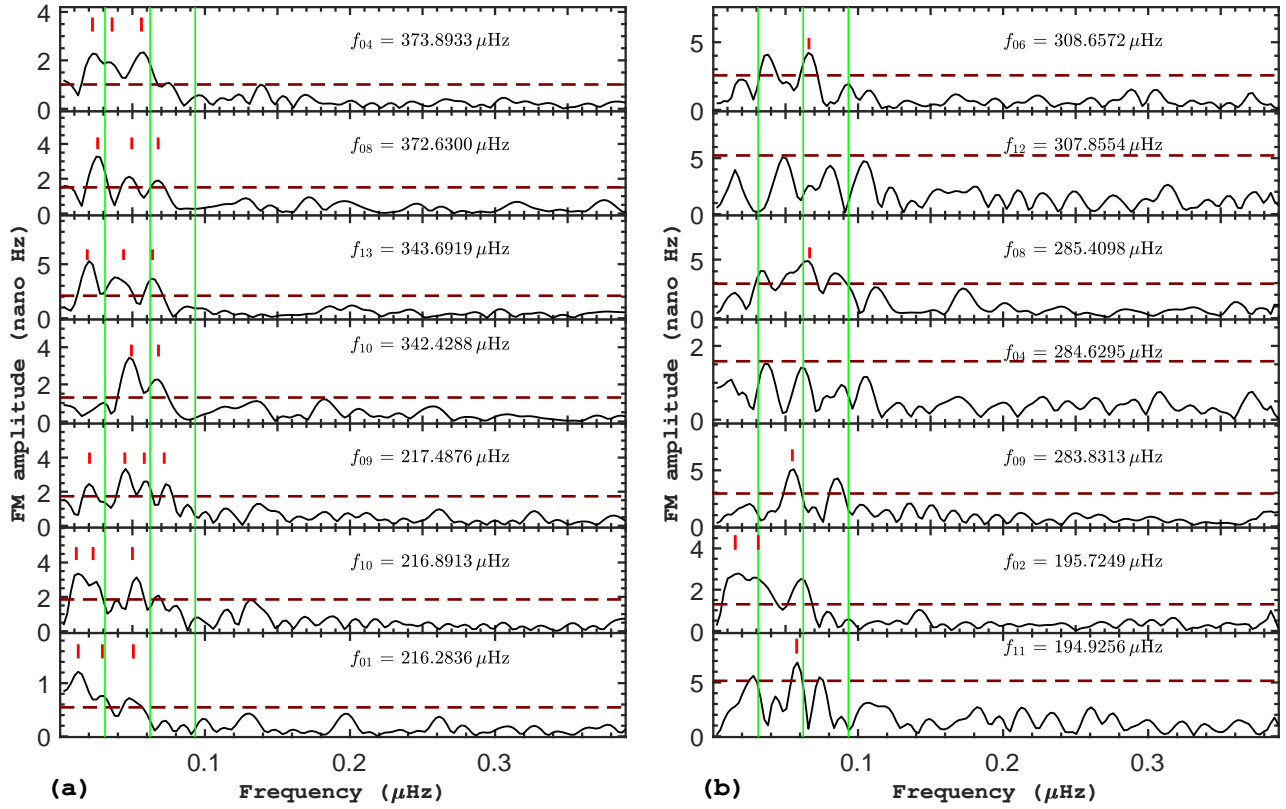


Figure 11. The LSPs of frequency modulations concentrating on the representative frequencies in KIC 2438324 (a) and KIC 11179657 (b). The Vertical line indicates the *Kepler* orbital frequency, $f_K = 0.0311 \mu\text{Hz}$, and its harmonics. The dashed horizontal line represents the typical 4σ level of local noise. The detected frequencies above that level are found with the values where the vertical segments stand. Note that LSPs in (b) are resolved with sidelobes due to observation gaps.

theory predicts, similar timescales of FMs within the same multiplet are observed. Several resonant components, whose frequencies evolve in phase or anti-phase during the observations, show similar modulation patterns to those found between the components of the quintuplet Q_1 in KIC 3527751 (Paper I). We note that most of the FM timescales are not close to that of *Kepler*'s orbit and its resonances which was recently reported on phase modulations in non-Blazhko RR Lyrae stars (Benkó et al. 2019). However, the measured AMs, particularly in KIC 2438324, are contaminated by a systematic modulation pattern (discussed later) and by the correction of the light fraction associated to the target. This pollution can seriously impair the recovery of intrinsic amplitude modulation patterns of oscillation modes, which is the most straightforward way to characterize nonlinear effects on stellar pulsations. These systematic patterns will need to be removed prior to any detailed quantitative comparison with theoretical predictions. Our suggestion, in the meantime, is that stars without contaminating light should be given a higher priority for such studies. Finally, we point out that the modulations may become more complicated as the number of the detected frequency increases, comparing AMs and FMs detected in KIC 2438324, KIC 11179657, KIC 10139564 and KIC 3527751.

6.3. Instrumental effects?

At odds with what was found for the star KIC 3527751, we discovered systematic AM patterns in several independent modes and in the orbital signals of the two stars considered in this paper. The orbital signal, expected to be constant in amplitude, was used as a reference to calibrate intrinsic modulation patterns. This is the first time that this systematic is characterized to better measure AMs and FMs of oscillation modes in pulsating compact stars. In previous studies, we had not encountered this kind of modulation pattern although we had processed more than 300 frequencies (see Zong et al. 2016a,b, and Paper I). Systematic AMs are likely different from star to star, but they can be distinguished from the various AMs induced by nonlinear mode interactions. A key feature on these systematic modulations is that they have a timescale identical to *Kepler*'s orbital period, $P \sim 372.5$ days. Figure 12 shows a phase diagram constructed on the 372.5 d period for the AM of f_{orb} in KIC 2438324. The folded curves clearly show that the right period was used for the raw and corrected AMs (with different zero-points in phase). To confirm the period, we used the PDM (phase dispersion minimization) to evaluate the period, which gives a value of 372.7 d and 371.5 d for the raw and the

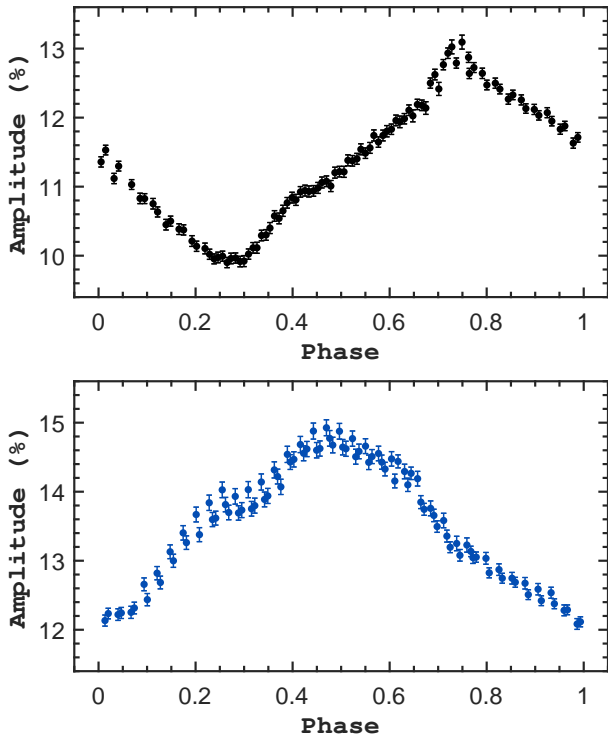


Figure 12. Phase diagram of the amplitude variation of the orbital frequency in KIC 2438324: (*Top* panel) raw flux and (*bottom* panel) corrected flux.

corrected AM, respectively. Similarly, a value of 373.1 d was obtained from a Lomb-Scargle periodogram of the raw AM curve. This modulation pattern of timescale identical to the orbital period of *Kepler* cannot be coincidental and is most likely induced by instrumental effects onboard.

This finding shows that one should be cautious when exploiting *Kepler*'s light curves to measure long-term amplitude modulations, particularly with periods near to the spacecraft orbit. For instance, a similar small-amplitude fluctuation was uncovered in M-giant stars based on *Kepler*'s photometry (Bányai et al. 2013), with several stars showing a systematic brightness variation on a *Kepler*-year timescale of unclear origin. Such variations can be harmful for many science objectives, such as determining the transit depth for wide-orbit exoplanets, which can be used to measure oblateness of transiting planets (see, e.g., Biersteker & Schlichting 2017). As the spacecraft rolls by 90 degrees every season, the fraction of contaminating light changes every quarter, which could possibly be related to the *Kepler*-year periodic AMs seen in KIC 2438324. However, the AMs are still showing a *Kepler*-year period (Figure 12) in the corrected fluxes, besides the fact that these have been rectified by the contamination factor. This indicates that the contamination factor may not be estimated precisely enough within and across quarters. In addition, quantum efficiency could also differ when stellar light is acquired from different pixels. Moreover, the point

spread function of the stars will also change as the telescope roll angle changes every quarter. Further investigation will need to be carried out with target pixel photometry, which may help us to remove this systematic amplitude variations. A plausible reason might be that the neighbour pixels around that target still contain a very small fraction of the flux (see, e.g., Pápics et al. 2017), meaning that we do not count the right amount of flux for the target when using the standard *Kepler*'s reduction pipeline. We finally recall that this kind of systematics in AMs needs to be given careful inspection also for the ongoing mission *TESS* (Ricker et al. 2014), especially for targets observed over several sectors.

6.4. General perspectives

Space missions, such as *Kepler* (Borucki et al. 2010) and *TESS* (Ricker et al. 2014), bring opportunities to measure frequencies in pulsating stars with accuracy of tens of micro Hz down to a few nano Hz. We are presently capable of measuring frequency variations on very tiny scales, allowing us to study new physics, such as how to precisely calculate FM patterns induced by nonlinear effects on pulsation modes. In particular, progress in this direction would allow to securely determine secular rates of frequency variations due to stellar evolution, or to detect with a higher confidence the presence of small orbiting objects, with residual modulations after the nonlinear FM correctly removed. This has received particular interest in compact pulsators these past decades, with the possibility to constrain the rate of pulsation period change (Kepler et al. 2005; Vauclair et al. 2011; Hermes et al. 2013) and uncover periodic phase variations caused by the presence of planetary companions (Silvotti et al. 2007, 2018). In the context of the two close binary systems KIC 2438324 and KIC 11179657 discussed in this paper, after correcting for the complex FMs due to nonlinear interactions, the residual modulation could also be used to measure the rate of spin-up induced by tides from the companion, if this acceleration is rapid enough, or set upper limits otherwise.

Even though flux can be measured with high precision from space instruments, consecutive long-term observations are not free of systematic uncertainties that can affect such measurements. We have shown that thorough inspections of the obtained amplitudes must be carried out if the goal is to characterize accurately amplitude variations over long timescales (to study, e.g., physics of nonlinear mode interactions inside stars in Goupil & Buchler 1994; Buchler et al. 1995). In the nonlinear physics context, any instrumental bias to the intrinsic values of AMs would lead to results far away from the real modulation patterns, which will likely affect the critical physical quantities from the calculations of amplitude equations.

7. CONCLUSION

In this paper, the second of a series devoted to a systematic survey of pulsations in evolved compact stars (hot B subdwarf and white dwarf stars) as observed from the *Kepler* spacecraft, we focus on the comparison of AMs and FMs of oscillation modes as measured from the two types of flux calibrations, raw and corrected, delivered by the standard data reduction pipeline. This is done for two pulsating sdB stars, KIC 2438324 and KIC 11179657, which are both primary components of a binary system. The first goal was to precisely measure the intrinsic AMs and FMs of oscillations in those compact stars, further paving the way to theoretical and quantitative calculations within the framework of nonlinear stellar oscillation theory that could rely on such observations.

We first extended our estimation of uncertainties in measuring amplitudes and frequencies by testing 50 000 artificial signals, a large improvement over the more limited set of 1000 signals originally used by Zong et al. (2016b). These new simulations agree well with the previous results of Zong et al. (2016b), and demonstrates amplitude and frequency errors all are measured accurately, independent of the S/N ratio of the signal. However, uncertainties in the phase determination may be overestimated depending on S/N ratio (Figure 1). The latter, however, are not used for our objectives, yet. With these quantitative tests, we could precisely and confidently extract frequencies from the light curves of the two sdB stars using the two different flux calibrations, raw (SAP) and corrected (PDC-SAP). Since the photometry is longer than that in previous published literature about these objects, we were able to resolve 22 and 34 frequencies in KIC 2438324 (Table 1) and KIC 11179657 (Table 2), respectively. These bring an additional four and eight low amplitude modes to the formerly available lists of detected pulsations in these stars. We mention that both stars show very similar and relative simple frequency contents, and could be of high interest for future comparative seismic analyses.

We then precisely measured AMs/FMs for frequencies with amplitude down to ~ 0.7 ppt and ~ 0.3 ppt in KIC 2438324 and KIC 11179657, respectively. By comparing modulation patterns measured from two different kinds of flux, we find that AM patterns change significantly for the modes observed in KIC 2438324, which suffer from significant light contamination by nearby stars (Figure 8), but not for the modes in KIC 11179657 whose contamination factor is almost zero (Figure 10). Differing from our previous studies, we identify clear systematic AMs of frequencies in KIC 2438324 through inspection on many independent modes and binary signals. Several methods have been used to determine the timescale of this regular AM, leading to a periodicity of about 372.5 days which is identical to *Kepler*'s orbital period around the Sun (Figure 12). We argue that this systematic AM is an additional difficulty, which to

some extent can impair an accurate determination of the intrinsic AMs needed to constrain theoretical calculations of nonlinear couplings of pulsation modes, but also, more generally, for the study of long-period variables or transiting exoplanets. However, we stress that this effect can be corrected provided that some reference of normally constant amplitude exist, which is the case for pulsating stars in binary systems. In summary, these findings suggest that stars without contamination could be much easier to rectify the systematic AMs because the correction of light pollution could destroy the real AM patterns.

Although the AMs evolve following different patterns in KIC 2438324, the FM patterns are found to be unaffected from these two independent measurements with different types of flux. All the representative frequencies exhibit frequency variations in a relative narrow scale (Figure 4-7), typically of 10-20 nano Hz, which is of the same order as the frequency mismatch found in the triplets at $217 \mu\text{Hz}$ in KIC 2438324 (Figure 4) and $284 \mu\text{Hz}$ in KIC 11179657 (Figure 6). These FMs show somewhat (anti-)correlations between different components within the same multiplet, with peak-to-peak periodicities ranging from months to years. This suggests that nonlinear weak mode interaction happens between the involved components, as expected from the nonlinear mode coupling theory (e.g., Buchler et al. 1995). We recall that similar results have been obtained in our previous studies, such as in KIC 3527751 (Paper I). Observation of these FMs are of particular interest for future comparisons with nonlinear calculations using, e.g., the amplitude equation formalism (Goupil & Buchler 1994).

In forthcoming steps, we will concentrate on the other pulsating sdB stars with appropriate data available for such kind of study in order to provide a more general statistical view on these modulations. We stress that the comparison described in this paper also applies to the photometry gathered from the *TESS* mission, since these data are processed through a very similar pipeline to the one used for *Kepler* (Jenkins et al. 2016). We expect that AMs/FMs of oscillation modes in compact pulsators from *Kepler* observations, as well as from the ongoing *TESS* monitoring (Charpinet et al. 2019), will ultimately provide a solid base for future theoretical investigations of nonlinear effects in stellar pulsations which may lead to new insight in the physics of stars and their oscillations, through, e.g., the determination of linear growth rates of modes.

Facility: *Kepler*

Software: FELIX (Charpinet et al. 2010)

ACKNOWLEDGMENTS

W.Z. acknowledges support from the National Natural Science Foundation of China (NSFC) through the grant 11903005 and 11833002, and the support from the Fundamental Research Funds for the Central Universities. S.C. and G.V. acknowledge support from the Agence Nationale de la Recherche (ANR, France) under grant ANR-17-CE31-0018, funding the INSIDE project, and financial support from the Centre National d'Études Spatiales (CNES, France). The authors gratefully acknowledge the *Kepler* team and all who have contributed to making this mission possible. Funding for the *Kepler* mission is provided by NASA's Science Mission Directorate.

REFERENCES

- Bányai, E., Kiss, L. L., Bedding, T. R., et al. 2013, *MNRAS*, 436, 1576
- Benkő, J. M., Jurcsik, J., & Derekas, A. 2019, *MNRAS*, 485, 5897
- Biersteker, J., & Schlichting, H. 2017, *AJ*, 154, 164
- Borucki, W. J., Koch, D., Basri, G., et al. 2010, *Science*, 327, 977
- Buchler, J. R., Goupil, M.-J., & Hansen, C. J. 1997, *A&A*, 321, 159
- Buchler, J. R., Goupil, M. J., & Serre, T. 1995, *A&A*, 296, 405
- Charpinet, S., Brassard, P., Fontaine, G., et al. 2019, *A&A*, 632, 90
- Charpinet, S., Fontaine, G., Brassard, P., Green, E. M., & Chayer, P. 2005a, *A&A*, 437, 575
- Charpinet, S., Green, E. M., Baglin, A., et al. 2010, *A&A*, 516, L6
- Charpinet, S., Van Grootel, V., Reese, D., et al. 2008, *A&A*, 489, 377
- Charpinet, S., Van Grootel, V., Fontaine, G., et al. 2011, *A&A*, 530, A3
- Deeming, T. J. 1975, *Ap&SS*, 36, 137
- Dziembowski, W. 1982, *AcA*, 32, 147
- Goupil, M.-J., & Buchler, J. R. 1994, *A&A*, 291, 481
- Goupil, M. J., Dziembowski, W. A., & Fontaine, G. 1998, *Baltic Astronomy*, 7, 21
- Hermes, J. J., Montgomery, M. H., Mullally, F., Winget, D. E., & Bischoff-Kim, A. 2013, *ApJ*, 766, 42
- Jenkins, J. M., Caldwell, D. A., Chandrasekaran, H., et al. 2010, *ApJL*, 713, L87
- Jenkins, J. M., Twicken, J. D., McCauliff, S., et al. 2016, *Proc. SPIE*, 9913, 99133E
- Kovacs, G., & Buchler, J. R. 1989, *ApJ*, 346, 898
- Kepler, S. O., Costa, J. E. S., Castanheira, B. G., et al. 2005, *ApJ*, 634, 1311
- Montgomery, M. H., & Odonoghue, D. 1999, *Delta Scuti Star Newsletter*, 13, 28
- Murphy, S. J. 2012, *MNRAS*, 422, 665
- Lee, J. W., Kim, S.-L., Kim, C.-H., et al. 2009, *AJ*, 137, 3181
- Lomb, N. R. 1976, *Ap&SS*, 39, 447
- Østensen, R. H., Silvotti, R., Charpinet, S., et al. 2010, *MNRAS*, 409, 1470
- Pablo, H., Kawaler, S. D., & Green, E. M. 2011, *ApJL*, 740, L47
- Pablo, H., Kawaler, S. D., Reed, M. D., et al. 2012, *MNRAS*, 422, 1343
- Reed, M. D., Baran, A., Østensen, R. H., Telting, J., & O'Toole, S. J. 2012, *MNRAS*, 427, 1245
- Scargle, J. D. 1982, *ApJ*, 263, 835
- Pápics, P. I., Tkachenko, A., Van Reeth, T., et al. 2017, *A&A*, 598, A74
- Ricker, G. R., Winn, J. N., Vanderspek, R., et al. 2014, *Proc. SPIE*, 9143, 914320
- Silvotti, R., Schuh, S., Janulis, R., et al. 2007, *Nature*, 449, 189
- Silvotti, R., Schuh, S., Kim, S.-L., et al. 2018, *A&A*, 611, A85
- Vauclair, G., Fu, J.-N., Solheim, J.-E., et al. 2011, *A&A*, 528, A5
- Zong, W., Charpinet, S., Fu, J.-N., et al. 2018, *ApJ*, 853, 98
- Zong, W., Charpinet, S., & Vauclair, G. 2016b, *A&A*, 594, A46
- Zong, W., Charpinet, S., Vauclair, G., Giammichele, N., & Van Grootel, V. 2016a, *A&A*, 585, A22